

# Single current sensor based fault tolerant control of interior permanent magnet synchronous machine for drive applications

Sankhadip Saha<sup>1</sup>, Urmila Kar<sup>2</sup>

<sup>1</sup>Department of Electrical Engineering, Netaji Subhash Engineering College, Kolkata, India

<sup>2</sup>Department of Education and Management, National Institute of Technical Teachers' Training and Research, Kolkata, India

## Article Info

### Article history:

Received Mar 2, 2022

Revised Jul 27, 2022

Accepted Aug 26, 2022

### Keywords:

Current sensor  
Electric Vehicle  
Fault-tolerant control  
Field-oriented control  
Interior permanent magnet synchronous machine

## ABSTRACT

This paper presents an integrated method for current sensor fault detection and fault tolerant control (FTC) for traction interior permanent magnet synchronous motor (IPMSM). The proposed current sensor fault detection method is based on detecting changes in the d-q axis current. The FTC is based on d-q axis current estimation from the reference d-q axis current and the phase current measured by the surviving current sensor. The current estimation process is independent of machine parameters. Hence the estimation is robust and requires less computational cost. The effectiveness of the FTC method is verified by the transient analysis. Such FTC is suitable for electric vehicle traction applications to ensure non-stop control operation of the drive in the entire range of speed. The efficacy of the proposed FTC method is tested through extensive simulations in MATLAB/Simulink environment. The real-time applicability of the proposed FTC method using the cost-effective digital signal processor (DSP) is verified on Texas Instruments© TMSF28379D through the processor in loop (PIL) simulation model.

*This is an open access article under the [CC BY-SA](https://creativecommons.org/licenses/by-sa/4.0/) license.*



## Corresponding Author:

Sankhadip Saha

Department of Electrical Engineering, Netaji Subhash Engineering College  
Mauza Ranabhatia, Techno City, Garia, Kolkata, West Bengal 700152, India

Email: sankhadip.saha@nsec.ac.in

## 1. INTRODUCTION

In recent times, interior permanent magnet synchronous motor (IPMSM) has drawn major attention in traction applications, particularly in electric vehicle (EV) propulsion systems [1]. As compared to its other counterpart i.e. surface permanent magnet synchronous motor (SPMSM), IPMSM is preferred for its salient features such as high power density, high efficiency and better field weakening capability for constant power operation, which is a typical case for electric traction system [2]. IPMSM drive employs closed-loop control for high-performance vector control implementation, which in turn requires one position and at least two current sensors [3].

The most important safety requirement in the traction drive system demands an unbroken control loop for nonstop motor operation, even in a faulty sensor system. Therefore, the electric vehicle safety research nowadays focuses greatly on fault detection and fault tolerant control (FTC) of the drive system. Nonetheless, the studies on fault detection and reconfiguration techniques have found that most of the research work is based on motor winding faults [4]–[6] and inverter switch faults [7]–[9].

Another reason for control loop failure of IPMSM drive is due to malfunction of the feedback loop sensors employed for outer loop speed and internal loop current control [10]. Fault detection and tolerant control techniques are reported for only speed sensor fault [11], [12], for only current sensor fault [13], [14]

and for both speed and current sensor faults [15], [16]. Sensor fault detection techniques generally are of three types i.e. signal-based [7], [17], model-based [16], [18], [19] and knowledge-based [20].

Kommuri *et al.* [19], explained a robust fault detection scheme based on a bank of higher order sliding mode (HOSM) observer to detect position, voltage and current sensor fault in a PMSM drive. Because of its several advantages over rotational permanent magnet synchronous motors, the primary permanent magnet linear motors are generally used for subway applications [14]. Current sensor fault detection and isolation for vector control of induction motor drives is proposed in [10], where the elementary concept on axis transformation is introduced. The efficacy of the proposed method is justified with respect to transient and steady-state performance and verified with the experimental results. In post-fault operation, motor phase currents can also be reconstructed from a single dc-link current sensor [21] which is rarely mounted in PMSM drive system. Moreover, without proper sampling of dc link current, current reconstruction may not be successful. Speed sensor-less field-oriented control of PMSMs is possible using a nonlinear sliding mode observer, which utilizes two current sensor information. A fault tolerant control scheme based on current space vector error reconstruction is proposed in [22] for the PMSM drive.

From the foregoing discussion, it is clear that the severity of the current sensor fault is significant in traction application as it requires a multi-motor drive system [14]. Through an extensive literature survey on current sensor fault detection and localization techniques [7], [13], [17], it has been found that sensor fault detection time is a function of motor current fundamental period and varies depending on the speed and torque demand of the drive. Hence, two important points emerge in the context of current sensor fault detection. Firstly, the detection time should be fast, and secondly, the detection time should be irrespective of the drive operating condition. Current sensor fault remedial measure is also a challenging task for ensuring successful FTC of the drive. Several extensive FTC studies have also been carried out on induction motor drives [10], [23]–[26]. Survival control strategies are adopted either by switching closed loop to open loop [23], [25] or continuing closed loop operation by the corresponding signal from the available observer [10], [19], [27]. Unlike in case of induction motor, the first fault tolerant survival control strategy as mentioned above is not suitable for synchronous motor drives due to instability and loss of synchronism [28]. Hence the FTC method for PMSM drive should be robust and independent of the motor model, which is an important consideration in this paper. Even more important requirement for FTC of the drive is that detection of faulty current sensor and its reconfiguration should be integrated with the drive control system for faster switching from normal operation to FTC.

This paper presents a simple but effective fault tolerant control method using only one surviving current sensor for a 100 KW IPMSM traction system which utilizes the maximum torque per ampere (MTPA) algorithm. The performance of the proposed method is investigated under various test circumstances and sensor fault conditions applicable for electric vehicle traction systems. Moreover, a processor in loop (PIL) test using the cost-effective digital signal processor (DSP) (TMSF28379D) is conducted to demonstrate the real-time viability of the proposed method.

## 2. MATHEMATICAL MODEL OF IPMSM

The mathematical model of IPMSM can be derived by neglecting hysteresis loss, eddy current loss and saturation while considering the induced emf as sinusoidal. However, the effect of saturation can be taken into account with parameter changes. The voltage equations for IPMSM in rotating reference frame (d-q) can be modelled as given in (1), where  $R_s$  is the stator resistance,  $L_d$  and  $L_q$  are the stator inductances in the d-q axis,  $\omega_e$  is the rotor electrical speed,  $\theta_e$  is rotor electrical position,  $\Psi$  is the magnetic flux linkage,  $p$  is the number of pole pairs, and  $\rho$  is the derivative operator.

$$\begin{bmatrix} V_d \\ V_q \end{bmatrix} = \begin{bmatrix} R_s + \rho L_d & -\omega_e L_q \\ \omega_e L_d & R_s + \rho L_q \end{bmatrix} \begin{bmatrix} I_d \\ I_q \end{bmatrix} + \begin{bmatrix} 0 \\ \omega_e \psi \end{bmatrix} \quad (1)$$

The (1) can be rewritten in the form of (2), where the second term of the equation is the expression for extended back emf (EEMF).

$$\begin{bmatrix} V_d \\ V_q \end{bmatrix} = \begin{bmatrix} R_s + \rho L_d & -\omega_e L_q \\ \omega_e L_d & R_s + \rho L_d \end{bmatrix} \begin{bmatrix} I_d \\ I_q \end{bmatrix} + \begin{bmatrix} 0 \\ \{\omega_e[(Ld - Lq)I_d + \psi] + (Ld - Lq)(\rho I_q)\} \end{bmatrix} \quad (2)$$

The (2) is transformed to (3) in the stationary reference frame ( $\alpha$ - $\beta$ )

$$\begin{bmatrix} V_\alpha \\ V_\beta \end{bmatrix} = \begin{bmatrix} R_s + \rho L_d & -\omega_e(L_q - L_d) \\ \omega_e(L_q - L_d) & R_s + \rho L_d \end{bmatrix} \begin{bmatrix} I_\alpha \\ I_\beta \end{bmatrix} + \left\{ \omega_e[(L_d - L_q)I_d + \psi] + (L_d - L_q)(\rho I_q) \right\} \begin{bmatrix} -\sin\theta_e \\ \cos\theta_e \end{bmatrix} \quad (3)$$

The torque equation of IPMSM is given below in (4).

$$T = 1.5[P_p\psi I_q + P_p\omega_e(L_d - L_q)I_d I_q] \quad (4)$$

### 3. FAULT TOLERANT CONTROL SYSTEM OF IPMSM

The fault tolerant control (FTC) design employs a field-oriented control (FOC) approach to improve electric motor efficiency and enable motors to operate at optimum torque. The precise and quick speed control of FOC is suitable for applications with dynamic load fluctuations such as electric vehicles. The FTC architecture is illustrated in Figure 1. The fault diagnosis part is also embedded in the drive control system.

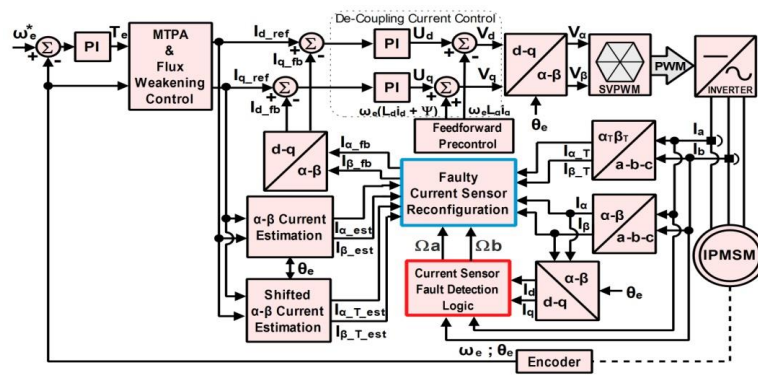


Figure 1. Fault tolerant control system model

#### 3.1. Controller model of IPMSM

Considering the traction application, control algorithm may be employed to run the IPMSM below and above the base speed as desired. In field-oriented control, IPMSM runs maximum up to base speed which is limited by the back emf, rated current and stator voltage of the motor. However, field weakening control is implemented over the base speed by setting negative d-axis current, which in turn again reduces flux linkage. Depending on the torque-current characteristic of the IPMSM, the reference d-axis current also limits the reference q-axis current, limiting the motor torque. Therefore, the motor operation slides from the constant torque region under the base speed to the constant power region over the base speed with a limited torque capability.

Considering the inverter current and voltage constraints, the motor phase current  $I_a$  and the motor terminal voltage  $V_a$  are defined as (5) and (6).

$$I_a = \sqrt{I_d^2 + I_q^2} \leq I_m \quad (5)$$

$$V_a = \sqrt{V_d^2 + V_q^2} \leq V_m \quad (6)$$

Where,  $I_m$  is maximum tolerable phase current at ambient temperature and  $V_m$  is maximum available terminal voltage of the inverter. The reference  $V_d$  and  $V_q$  are computed by (7) and (8).

$$V_d = -\omega_e L_q i_q \quad (7)$$

$$V_q = \omega_e (L_d i_d + \psi) \quad (8)$$

The presence of saliency ( $L_d < L_q$ ) in the rotor circuit of IPMSM produces reluctance torque in addition to the electromagnetic torque. Therefore, the maximum torque can be achieved in the constant torque region by calculating optimal current values of  $I_{d\_mtpa}$  and  $I_{q\_mtpa}$  from the torque equation according to the maximum torque per ampere (MTPA) algorithm [29].

$$i_{d\_mtpa} = \frac{\psi}{4(L_q - L_d)} - \sqrt{\frac{\psi^2}{16(L_q - L_d)^2} + \frac{I_m^2}{2}} \tag{9}$$

$$i_{q\_mtpa} = \sqrt{I_m^2 + I_{d\_mtpa}^2} \tag{10}$$

Therefore, the field weakening current values of  $I_{d\_fw}$  and  $I_{q\_fw}$  are derived from (7)–(8) and satisfying the relation of (6).

$$i_{d\_fw} = -\frac{\psi}{L_d} + \frac{1}{L_d} \sqrt{\frac{V_d^2}{\omega_e^2} - (L_q i_q)^2} \tag{11}$$

$$i_{q\_fw} = \sqrt{I_m^2 + I_{d\_fw}^2} \tag{12}$$

Due to large inductance, IPMSM has significant cross-coupling effect which even becomes worse in the field weakening region as the speed increases. Hence the cross-coupling effect needs to be cancelled. In order to improve the overall current transient response, the d-axis and the q-axis currents are decoupled via feed-forward pre-control.

$$V'_d = U_d - \omega_e L_q i_q \tag{13}$$

$$V'_q = U_q + \omega_e (L_d i_d + \psi) \tag{14}$$

### 3.2. Current sensor fault detection

Two physical current sensors (for phase-A and phase-B) are the minimum required for the successful operation of the drive since the remaining phase current (phase-C) can be calculated mathematically. According to Figure 2, the measured a-b-c phase currents are first converted into  $\alpha$ - $\beta$  axis currents and then converted to d-q axis currents by the clark transformation and park transformation, respectively.

The key idea behind the fault detection logic is the change detection in the d-q axis current for any sudden change in the measured a-b phase current. With the advancement of real-time MCUs and fast current loop technology, the current loop bandwidth can be increased to a large value that yields a very short sampling time for current loop calculation. The sampling interval is thus much shorter than the electrical time constant. The speed loop bandwidth is also lower than the current loop bandwidth. Therefore, the electrical speed can be considered as almost constant and the motor current varies almost linearly during the entire sampling interval. The d-q axis current sample values are compared with the previous sample values. The d-q axis current at sampling interval (n+1) will just somewhat deviate from the previous sample when both the current sensors are working properly. On the flip side, though, the deviation turns out to be larger when any one of the current sensors becomes faulty. Aiming to comprise both the d-q coordinates, the sum of the squared magnitude of the current error vector is considered as the current residual ( $\mathcal{E}_r$ ) for further logical comparison with respect to a preset threshold. The value of the current residual is very high during the faulty sensor condition and comparatively low otherwise. Hence, for any of the current sensor failure either at any phase, the logic comparator ( $>$ ) gives a high signal to the corresponding S-R flip-flop in that phase.

It is vital to be noted here that there is no definite way to determine the threshold value since it depends on the operating point of the drive. In a healthy system, the current residual always lies within the expected range, so the threshold value is set by a few trial-and-error runs. However, the threshold value is load-dependent, and it is difficult to set the threshold at a light load. To encounter this loading problem, a simple adaptive threshold ( $\lambda_{th}$ ), as a function of 1% of  $I_q$  current is selected in our case as  $I_q$  current depends on the load. In addition, the absolute values of the current signals in each phase are also kept under the scanner by another logical comparator that verifies whether the signal value is zero ( $I_{th}$ ) or not at the instant of fault in the corresponding phase. Instead of exact zero value,  $I_{th}$  is chosen carefully considering sensor noise. On the occurrence of any of the current sensor faults, both the high signals from the first S-R latch and

the corresponding logical operator ( $=$ ) are further processed by an AND logic for the final output. As a consequence, the misfiring probability by the fault detection logic can be cancelled out. The outputs from the AND logic of each phase are given to a pair of two cross coupled S-R latches. Finally, the outputs of the two cross coupled S-R latches ( $\Omega_a, \Omega_b$ ) are linked to the current sensor fault reconfiguration module. The high value of any of the two cross coupled S-R latches ( $\Omega_a, \Omega_b$ ) indicate the corresponding phase current sensor fault.

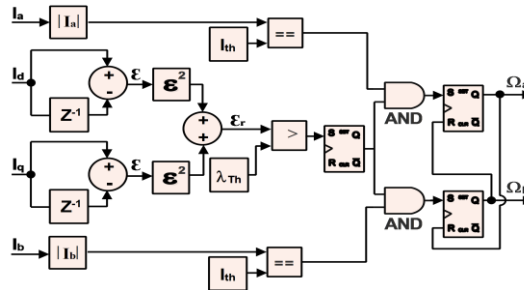


Figure 2. Current sensor fault detection logic

**3.2.1. Reconfiguration of faulty current sensor**

The IPMSM speed control system model mainly includes three PI controllers. One PI controller is employed for outer loop speed control, whereas the other two PI controllers are employed for inner loop current control in the d-axis and q-axis, respectively. The process of reference d-q axis current generation is discussed in section 3.1. However, the feedback d-q axis currents are obtained by transforming three-phase (a-b-c) current to two-phase ( $\alpha\beta$ ) current using clark transformation and then  $\alpha\beta$  phase current to d-q axis current using park transformation. In space distribution, generally, the  $\alpha$ -axis is aligned with the a-phase, and the corresponding clark transformation is given by (15). If the  $\alpha$ -axis is shifted by  $120^\circ$  anticlockwise to be aligned with the b-phase as shown in Figure 3, the clark transformation, in this case, is given by (16).

$$\begin{bmatrix} I_\alpha \\ I_\beta \end{bmatrix} = \begin{bmatrix} 1 & 0 \\ \frac{1}{\sqrt{3}} & \frac{2}{\sqrt{3}} \end{bmatrix} \begin{bmatrix} I_a \\ I_b \end{bmatrix} \tag{15}$$

$$\begin{bmatrix} I_{\alpha\_T} \\ I_{\beta\_T} \end{bmatrix} = \begin{bmatrix} 0 & 1 \\ -\frac{2}{\sqrt{3}} & -\frac{1}{\sqrt{3}} \end{bmatrix} \begin{bmatrix} I_a \\ I_b \end{bmatrix} \tag{16}$$

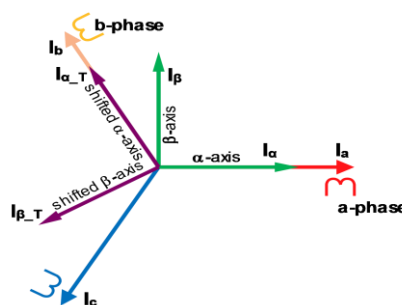


Figure 3. Space distribution of  $\alpha$ -axis and shifted  $\alpha$ -axis

From (15) and (16), it is clear that the  $\alpha$ -axis current and the shifted  $\alpha$ -axis current are dependent only on the a-phase current and the b-phase current, respectively. Therefore, the  $\alpha$ -axis current can always be regulated in case of either current sensor failure, no matter which phase is faulty. Hence, for the fault tolerant control action, only the  $\beta$ -axis current is needed to be estimated. If the control system is well designed that satisfies all transient and steady-state criteria of the IPMSM drive, then the  $\beta$ -axis current can be estimated from the reference d-q axis current [10], which is represented by (17) and (18).

$$\begin{bmatrix} I_{\alpha\_est} \\ I_{\beta\_est} \end{bmatrix} = \begin{bmatrix} \cos\theta_e & -\sin\theta_e \\ \sin\theta_e & \cos\theta_e \end{bmatrix} \begin{bmatrix} I_{d\_ref} \\ I_{q\_ref} \end{bmatrix} \tag{17}$$

$$\begin{bmatrix} I_{\alpha\_T\_est} \\ I_{\beta\_T\_est} \end{bmatrix} = \begin{bmatrix} \cos(\theta_e - 30^\circ) & -\sin(\theta_e - 30^\circ) \\ \sin(\theta_e - 30^\circ) & \cos(\theta_e - 30^\circ) \end{bmatrix} \begin{bmatrix} I_{d\_ref} \\ I_{q\_ref} \end{bmatrix} \tag{18}$$

Depending upon the operational status of both the current sensors as described in Table 1, continuity of the feedback  $\alpha$ - $\beta$  axis current can be maintained by the faulty current sensor reconfiguration unit, once the particular current sensor fault is identified by the fault detection unit. It is to be noted here that fault-tolerant operation will not work when both the current sensors become faulty. Thus, the operating principle of the faulty current sensor reconfiguration unit can be depicted as shown in Figure 4 and as represented by the generalized form as (19) and (20).

$$I_{\alpha\_fb} = I_\alpha + \Omega_a(I_{\alpha\_T} - I_\alpha) \tag{19}$$

$$I_{\beta\_fb} = \Omega_a(I_{\beta\_T\_est} - I_\beta) + \Omega_b(I_{\beta\_T\_est} - I_\beta) + (1 + \Omega_a\Omega_b)I_\beta \tag{20}$$

Table 1. Sensor diagnostics and feedback  $\alpha$ - $\beta$ -axis currents

a-phase current sensor	b-phase current sensor	Fault flag [ $\Omega_a, \Omega_b$ ]	$\alpha$ - $\beta$ -axis currents [ $I_{\alpha\_fb}, I_{\beta\_fb}$ ]
Healthy	Healthy	[0,0]	$I_\alpha \& I_\beta$
Healthy	Faulty	[0,1]	$I_\alpha \& I_{\beta\_est}$
Faulty	Healthy	[1,0]	$I_{\alpha\_T} \& I_{\beta\_T\_est}$

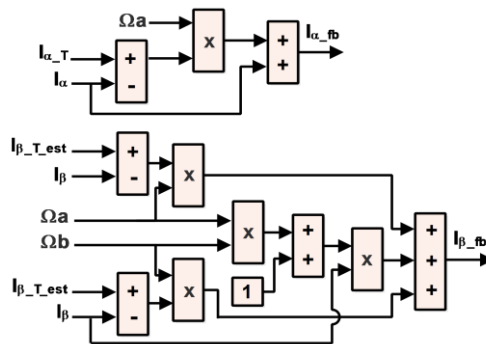


Figure 4. Faulty current sensor reconfiguration

### 3.2.2. Analysis of fault recovery transients

The current sensor reconfiguration module comes into effect immediately when the particular current sensor fault is detected. The occurrence of simultaneous faults in all the working sensors is not noticed in practice [30]. It is presumed here that the speed sensor is working properly during the current sensor fault. However, it is observed that there is a small transient in response during fault reconfiguration. Taking switching from normal d-q axis control to the shifted d-q axis control.

$$V_{d\_ftc} = V_d + \Delta V_d \tag{21}$$

$$V_{q\_ftc} = V_q + \Delta V_q \tag{22}$$

$$\theta_{d\_ftc} = \theta_e + \Delta\theta_e \tag{23}$$

Where  $\Delta V_d$  and  $\Delta V_q$  are the synchronous frame voltage differences.  $\Delta\theta_e$  is the phase difference between the pre-fault and the post-fault controller. Considering the d-axis aligning with the  $\alpha$ -axis, from inverse park transform, the corresponding  $V_\alpha$  and  $V_{\alpha\_ftc}$ .

$$V_\alpha = V_d \cos \theta_e - V_q \sin \theta_e \quad (24)$$

$$V_{\alpha\_ftc} = (V_d + \Delta V_d) \cos(\theta_e + \Delta \theta_e) - (V_q + \Delta V_q) \sin(\theta_e + \Delta \theta_e) \quad (25)$$

Thus, the change of  $V_\alpha$  when the FTC comes into action.

$$\Delta V_\alpha = V_{\alpha\_ftc} - V_\alpha = V_d [\cos \theta_{e\_ftc} - \cos \theta_e] - V_q [\sin \theta_{e\_ftc} - \sin \theta_e] - |\Delta V_s| \sin(\theta_{e\_ftc} - \varphi) \quad (26)$$

where

$$|\Delta V_s| = \sqrt{\Delta V_d^2 + \Delta V_q^2}, \varphi = \tan^{-1} \left( \frac{\Delta V_d}{\Delta V_q} \right) \quad (27)$$

For the encoder-based speed control loop, because of inertia, motor speed and angular position do not change suddenly at the instant of the current sensor fault. Therefore,  $\Delta V_\alpha = |\Delta V_s| \sin(\varphi - \theta_{e\_ftc})$ ;  $[\theta_{e\_ftc} = \theta_e]$ . Thus,  $\Delta V_\alpha$  depends on the difference between the magnitudes of the voltages before and after FTC. The  $\Delta V_d$  and  $\Delta V_q$ , in turn, depend on the change in output of the current controller on the d-axis and the q-axis, respectively. If the change in the d-q axis current can't be reduced quickly, the presented FTC approach may fail. According to (1), the d-axis and the q-axis currents are mutually coupled, i.e. any change in either axis (d or q) current may affect the other axis (d or q) current. To remove the current coupling effect, voltage decoupler is employed as given in (13) and (14) so that the d-axis and the q-axis voltage regulation becomes fast and independent. As a consequence, the current response may be improved, and the proposed FTC is fruitful.

#### 4. RESULTS FOR THE PROPOSED FTC METHOD

The proposed FTC method is verified on a 100 kW, 8-pole IPMSM drive setup developed in the MATLAB/Simulink environment. The machine parameters are listed in Table 2. The SVPWM switching frequency of the three-phase voltage source inverter is set to 20 kHz. It is worth mentioning that all the control signals are represented by per-unit (p.u) to create scalable control system laws. Since most of the DSPs use fixed point arithmetic and hence to improve the computational performance, the per unit representation is preferred over SI unit. Therefore, in terms of p.u representation, the motor parameters are calculated as base voltage = 167.4316 volt, base current = 517 amp, base speed = 3102 rpm and base torque = 220.5991 N-m. The control system always follows the MTPA scheme irrespective of the activation of the FTC mechanism. The controller parameters are given in Table 3.

Table 2. IPMSM specifications

Parameter	Value	Parameter	Value
Nominal Power ( $P_n$ )	100 Kw	Maximum Angular Velocity ( $\omega_m$ )	6500 rpm
Nominal Torque ( $T_n$ )	200 Nm	Nominal d-Axis Inductance ( $L_{d,n}$ )	0.00017416 H
Nominal DC link Voltage ( $V_{dc,n}$ )	290 V	Nominal q-Axis Inductance ( $L_{q,n}$ )	0.00029269 H
Nominal Permanent Magnet Flux ( $\psi_m$ )	0.0711	Stator Resistance ( $R_s$ )	0.0083 Ohm
Maximum Phase Current ( $I_m$ )	Wb	Number of Pole Pair ( $P_p$ )	4
	450A		

Table 3. Controller parameters

Controller	$K_p$	$K_i$
Speed Controller	8	90
d-axis Current Controller	3	100
q-axis Current Controller	3	100

Current sensor fault diagnosis performance is shown in Figure 5. It is presumed that the drive control system is started with all the sensors working properly. A complete outage of the b-phase current sensor occurs at  $t=10$ sec while the system is operating at rated speed with rated load. As shown in the zoomed portion of the first dashed box in Figure 5, the current sensor fault is detected at  $t=10.0001$  sec. Before the current sensor faulty condition, the current residual ( $\mathcal{E}_r$ ) is smaller than the preset threshold ( $\xi_{th}$ ). As shown in the zoomed portion of the second dashed box in Figure 5, at  $t=10$ sec, the current residual ( $\mathcal{E}_r$ ) is

increased from 0.00001 to 0.348, which is greater than the preset threshold. Consequently, the current sensor fault detection flag is enabled for switching to FTC operation.

In Figure 6, the FTC performance of the drive is evaluated at rated speed with rated load. The graph in Figure 6(a) shows that the drive control system can successfully switch to FTC after a b-phase current sensor fault at t=10 sec. Zoomed portion of Figure 6(b) shows the transient performance of the speed response. According to Table 1, the alpha-axis current ( $I_\alpha$ ) and the estimated beta-axis current ( $I_\beta$ ) are selected by the reconfiguration module for FTC, as shown in Figure 6(c) and Figure 6(d).

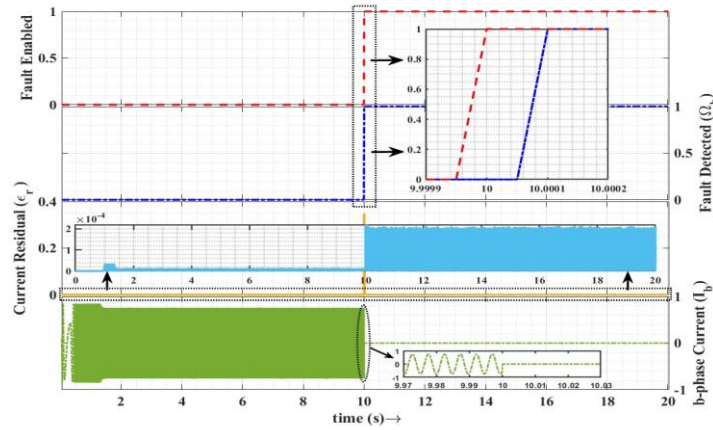


Figure 5. Performance of current sensor fault diagnosis

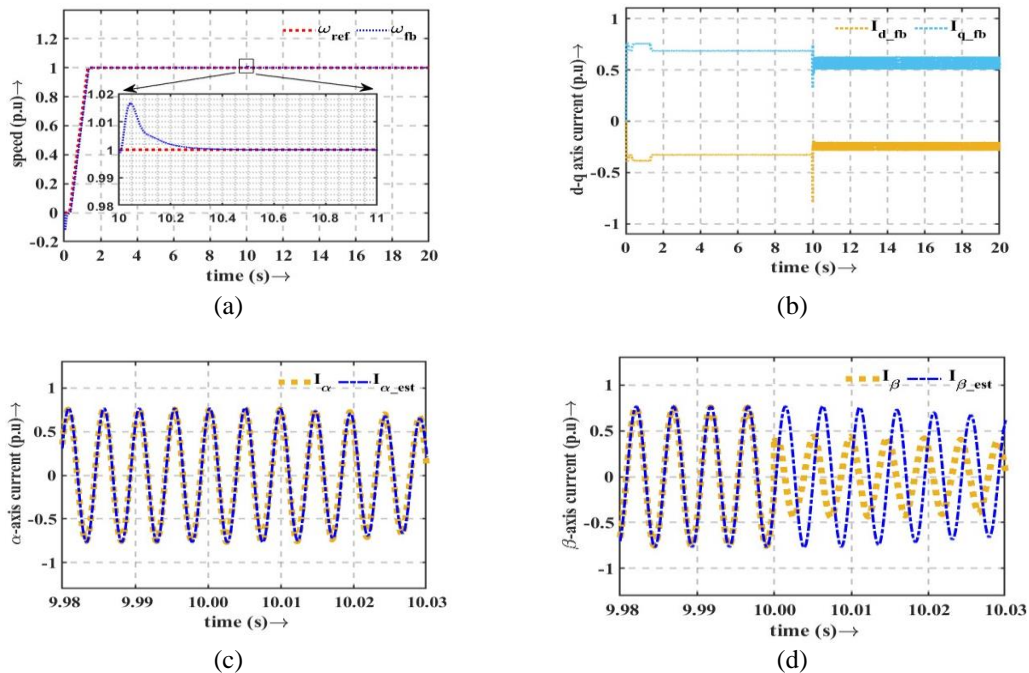


Figure 6. Evaluation of FTC performance at rated speed with rated load (a) speed control performance, (b) d-q axis current, (c)  $\alpha$ -axis current, and (d)  $\beta$ -axis current

Figure 7 shows the dynamic performance of the drive for ramp speed change under rated load post b-phase current sensor fault at t=3 sec. It is also seen that the single current sensor-based FTC takes over to continue the stable operation at a low speed of 0.1 p.u, as depicted in Figure 7(a), in Figure 7(b) d-q axis current, in Figure 7(c)  $\alpha$ -axis current and in Figure 7(d)  $\beta$ -axis current



The FTC designed for EV applications must be robust towards certain external load variations. Therefore, the proposed FTC method, evaluated for such an operating condition of the drive, is shown in Figure 8. When the drive is operating under no load, the b-phase current sensor becomes faulty at  $t=3\text{sec}$ , and FTC turns into operation  $t=3\text{ sec}$  onwards. Rated step load is applied and subsequently removed at  $t=5\text{sec}$  and  $t=10\text{sec}$ , respectively as shown in Figure 8(a) speed control performance, Figure 8(b) d-q axis current, Figure 8(c)  $\alpha$ -axis current, and Figure 8(d)  $\beta$ -axis current. The dynamic performance of the different operational conditions for all the cases mentioned above is given in Table 4.

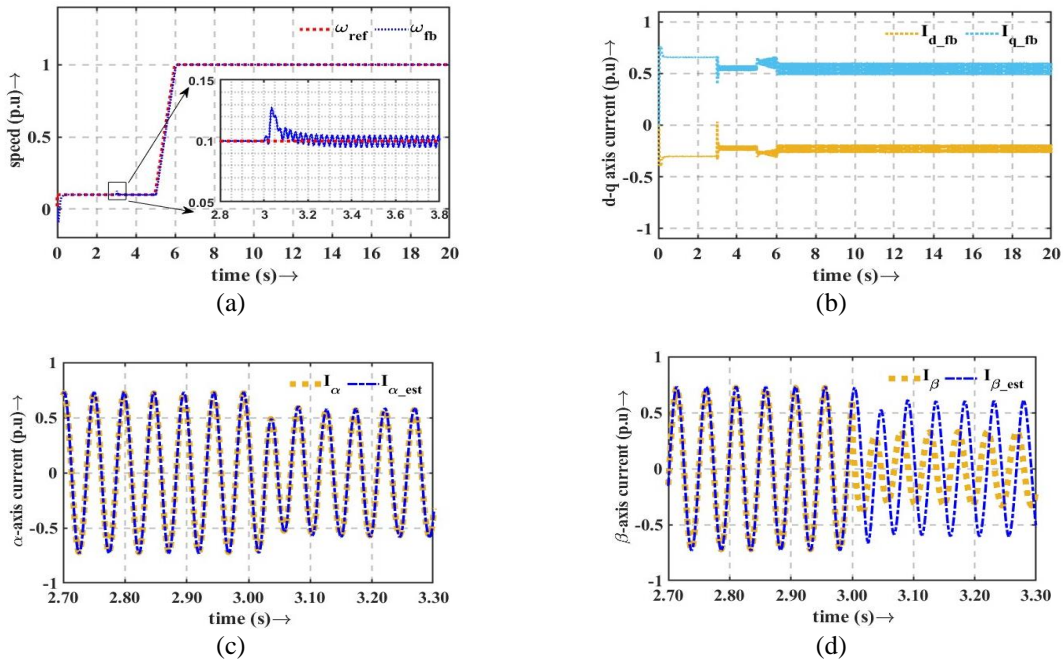


Figure 7. Evaluation of FTC performance during acceleration with rated load (a) speed control performance, (b) d-q axis current, (c)  $\alpha$ -axis current, and (d)  $\beta$ -axis current

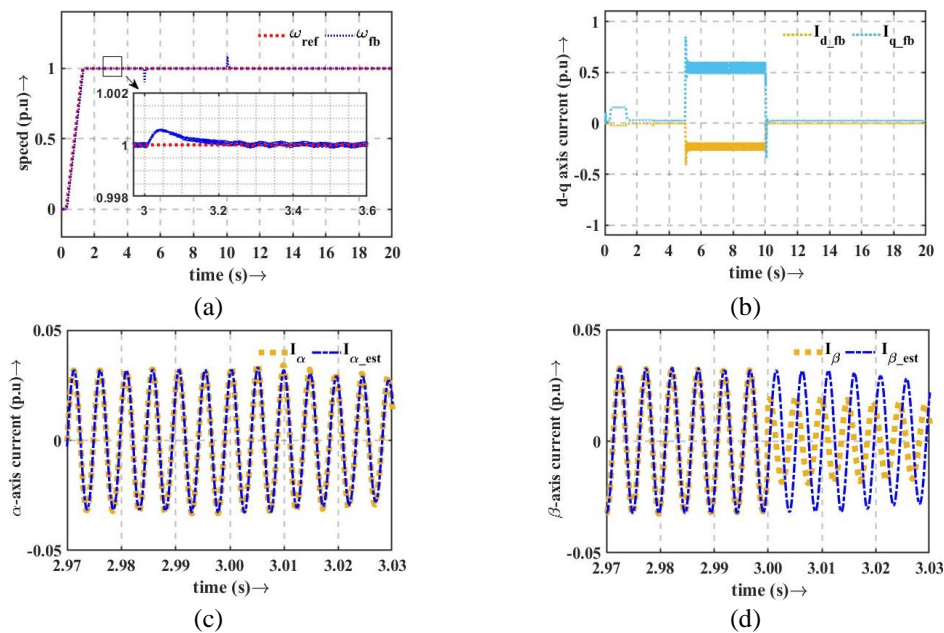


Figure 8. Evaluation of FTC performance sudden step load change (a) speed control performance, (b) d-q axis current, (c)  $\alpha$ -axis current, and (d)  $\beta$ -axis current

Table 4. Dynamic characteristic for FTC performance of the drive

Drive operating condition	Load application time (sec)	Current sensor fault occurring time (sec)	Current sensor fault detection time (sec)	Speed overshoot (%)	Speed undershoot (%)	Speed settling time (sec)
i) Rated speed with rated load	t= 0 sec	t= 10 sec	t= 10.0001 sec	< 2%	0 %	t= 10.4 sec
ii) Acceleration with rated load	t= 0 sec	t= 3 sec	t= 3.0001 sec	< 1.5 %	0 %	t= 3.4 sec
iii) Rated speed with step load (Load applied at t=5 sec & load removed at t=10 sec)	{ t= 5 sec t= 10 sec	t= 3 sec	t= 3.0001 sec	{ < 0.01 % 0% < 10%	{ 0 % < 11% 0 %	{ t= 3.3 sec t= 5.6 sec t= 10.6 sec

Like the current sensor fault detection performance, as depicted in Figure 5, the current sensor fault detection time for the last two cases (as depicted in Figures 7 and 8) is also found to be 0.0001 sec. It can also be noted that the proposed FTC is found fully applicable for a-phase current sensor fault. Hence, single current sensor-based continuous drive control can be ensured through by presented FTC method. Table 5 provides the nomenclature used in this paper.

Table 5. Nomenclature

Symbol	Parameter	Symbol	Parameter
$V_d, V_q$	The d-axis and q-axis stator voltages	$V_\alpha, V_\beta$	The $\alpha$ -axis and $\beta$ -axis stator voltages
$I_d, I_q$	The d-axis and q-axis stator currents	$I_\alpha, I_\beta$	The $\alpha$ -axis and $\beta$ -axis stator currents
$L_d, L_q$	The d-axis and q-axis inductances	$I_{\alpha\_est}$	The $\alpha$ -axis estimated stator current
$I_m$	The maximum phase current	$I_{\beta\_est}$	The $\beta$ -axis estimated stator current
$V_{dc}$	The nominal dc link voltage	$I_{\alpha\_T}$	The transformed $\alpha$ -axis stator current
$\Psi, P_p$	The magnetic flux linkage and the number of pole pair	$I_{\beta\_T}$	The transformed $\beta$ -axis stator current
$\omega_e^*$	The reference electrical speed	$I_{\alpha\_T\_est}$	The transformed $\alpha$ -axis estimated stator currents
$\omega_e, \theta_e$	The rotor electrical speed and the rotor electrical position	$I_{\beta\_T\_est}$	The transformed $\beta$ -axis estimated stator currents
$R_s, T_e$	The stator resistance and the electromagnetic Torque	$\Omega_a$	The a-phase current sensor fault detection flag
$P_n, T_n$	The nominal power and the nominal torque	$\Omega_b$	The b-phase current sensor fault detection flag

5. REAL-TIME VIABILITY WITH PIL TEST

From the literature survey [7], [10], [12], [17], [23], [24], it has been found that experimental validation of the drive control system often requires costly equipment with high sampling frequency like dSPACE, OPAL-RT and FPGA boards etc. To signify the real-time viability of the proposed fault-tolerant control method using cost-effective microprocessors, the PIL simulation test using the dual-core DSP TMSF28379D from Texas Instruments® is conformed. In the PIL testing framework, the embedded processor runs both the control loop and current sensor fault detection logic, whereas the part of the model, including the voltage source inverter, IPMSM, and feedback sensors, is implemented in MATLAB/Simulink. Although the DSP TMSF28379D is a 200 MHz dual-core processor, but only one core is utilized in the PIL test. The maximum execution time of the method is found to be 0.0093 ms (one iteration of the algorithm). To optimize the overall execution time, less critical functionalities like speed loop calculations can be moved to a slower rate of 200 Hz (one-tenth of current loop). Hence, current loop calculations and fault diagnostic module are executed at a sampling rate of 20 kHz. As a result, only 37% of the computational resources of one DSP core are used. Thus, the proposed fault tolerant control (FTC) method can be well implemented on inexpensive DSPs for real-time deployment. The experimental setup for the PIL arrangement is shown in Figure 9.

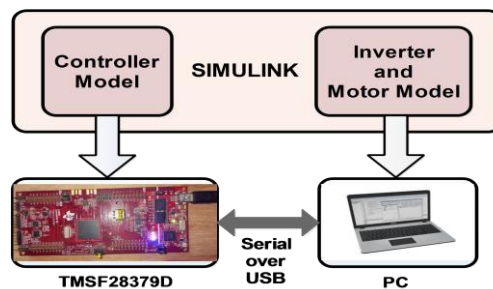


Figure 9. PIL experimental setup

## 6. CONCLUSION

The presented FTC method is capable of fail-safe non-stop operation of the IPMSM drive with only one healthy current sensor when the other current sensor becomes faulty. The drive control system follows the MTPA control scheme. To cancel the cross-coupling effect and to lower the saturation effect of current controllers during the faulty condition, decoupling feed-forward compensation is implemented to improve the transient performance. The speed tracking performance of the drive control system addresses issues related to the electric vehicle. In order to assess the feasibility of embedded controller implementation, PIL simulation is preferred nowadays for EV software testing. Therefore, the ability of the fault tolerant control to maintain uninterrupted operation of the IPMSM drive is verified experimentally through the extensive PIL simulation.




## REFERENCES

- [1] H. Elsherbiny, M. K. Ahmed, and M. A. Elwany, "Online efficiency optimization of IPMSM for electric vehicles," *International Journal of Power Electronics and Drive Systems (IJPEDS)*, vol. 12, no. 3, pp. 1369–1378, Sep. 2021, doi: 10.11591/ijped.v12.i3.pp1369-1378.
- [2] M. F. Omar, E. Sulaiman, M. Z. Ahmad, J. A. Rani, and A. CV, "Preliminary study of a new topology permanent magnet flux switching motor for electric buses," *Indonesian Journal of Electrical Engineering and Computer Science*, vol. 10, no. 2, pp. 446–455, May 2018, doi: 10.11591/ijeecs.v10.i2.pp446-455.
- [3] P. Q. Khanh and H. P. Huy Anh, "Advanced deep flux weakening operation control strategies for IPMSM," *International Journal of Electrical and Computer Engineering (IJECE)*, vol. 11, no. 5, pp. 3798–3808, Oct. 2021, doi: 10.11591/ijece.v11i5.pp3798-3808.
- [4] B. Sen and J. Wang, "Stator interturn fault detection in permanent-magnet machines using PWM ripple current measurement," *IEEE Transactions on Industrial Electronics*, vol. 63, no. 5, pp. 3148–3157, May 2016, doi: 10.1109/TIE.2016.2515560.
- [5] B. Wang, J. Wang, A. Griffio, and B. Sen, "Stator turn fault detection by second harmonic in instantaneous power for a triple-redundant fault-tolerant PM drive," *IEEE Transactions on Industrial Electronics*, vol. 65, no. 9, pp. 7279–7289, Sep. 2018, doi: 10.1109/TIE.2018.2793188.
- [6] R. Hu, J. Wang, A. R. Mills, E. Chong, and Z. Sun, "High-frequency voltage injection based stator interturn fault detection in permanent magnet machines," *IEEE Transactions on Power Electronics*, vol. 36, no. 1, pp. 785–794, Jan. 2021, doi: 10.1109/TPEL.2020.3005757.
- [7] I. Jlassi and A. J. M. Cardoso, "A Single Method for Multiple IGBT, Current, and Speed Sensor Faults Diagnosis in Regenerative PMSM Drives," *IEEE Journal of Emerging and Selected Topics in Power Electronics*, vol. 8, no. 3, pp. 2583–2599, Sep. 2020, doi: 10.1109/JESTPE.2019.2918062.
- [8] Q.-T. An, L.-Z. Sun, and L.-Z. Sun, "Current residual vector-based open-switch fault diagnosis of inverters in PMSM drive systems," *IEEE Transactions on Power Electronics*, vol. 30, no. 5, pp. 2814–2827, May 2015, doi: 10.1109/TPEL.2014.2360834.
- [9] S. Zerdani, M. L. Elhafyani, H. Fadil, and S. Zouggar, "Newly fault-tolerant indirect vector control for traction inverter," *International Journal of Power Electronics and Drive Systems (IJPEDS)*, vol. 12, no. 3, pp. 1576–1585, Sep. 2021, doi: 10.11591/ijped.v12.i3.pp1576-1585.
- [10] C. Chakraborty and V. Verma, "Speed and current sensor fault detection and isolation technique for induction motor drive using axes transformation," *IEEE Transactions on Industrial Electronics*, vol. 62, no. 3, pp. 1943–1954, Mar. 2015, doi: 10.1109/TIE.2014.2345337.
- [11] B. Tabbache, M. E. H. Benbouzid, A. Kheloui, and J.-M. Bourgeot, "Virtual-sensor-based maximum-likelihood voting approach for fault-tolerant control of electric vehicle powertrains," *IEEE Transactions on Vehicular Technology*, vol. 62, no. 3, pp. 1075–1083, Mar. 2013, doi: 10.1109/TVT.2012.2230200.
- [12] F. Mwasilu and J.-W. Jung, "Enhanced Fault-Tolerant Control of Interior PMSMs Based on an Adaptive EKF for EV Traction Applications," *IEEE Transactions on Power Electronics*, vol. 31, no. 8, pp. 5746–5758, Aug. 2016, doi: 10.1109/TPEL.2015.2495240.
- [13] N. M. A. Freire, J. O. Estima, and A. J. M. Cardoso, "A new approach for current sensor fault diagnosis in pmsg drives for wind energy conversion systems," *IEEE Transactions on Industry Applications*, vol. 50, no. 2, pp. 1206–1214, Mar. 2014, doi: 10.1109/TIA.2013.2271992.
- [14] W. Wang, Y. Feng, Y. Shi, M. Cheng, W. Hua, and Z. Wang, "Fault-tolerant control of primary permanent-magnet linear motors with single phase current sensor for subway applications," *IEEE Transactions on Power Electronics*, vol. 34, no. 11, pp. 10546–10556, Nov. 2019, doi: 10.1109/TPEL.2019.2899168.
- [15] S. K. Kommuri, S. Bin Lee, and K. C. Veluvolu, "Robust sensors-fault-tolerance with sliding mode estimation and control for PMSM drives," *IEEE/ASME Transactions on Mechatronics*, vol. 23, no. 1, pp. 17–28, Feb. 2018, doi: 10.1109/TMECH.2017.2783888.
- [16] A. B. Youssef, S. K. El Khil, and I. Slama-Belkhdja, "state observer-based sensor fault detection and isolation, and fault tolerant control of a single-phase PWM rectifier for electric railway traction," *IEEE Transactions on Power Electronics*, vol. 28, no. 12, pp. 5842–5853, Dec. 2013, doi: 10.1109/TPEL.2013.2257862.
- [17] C. Wu, C. Guo, Z. Xie, F. Ni, and H. Liu, "A signal-based fault detection and tolerance control method of current sensor for PMSM drive," *IEEE Transactions on Industrial Electronics*, vol. 65, no. 12, pp. 9646–9657, Dec. 2018, doi: 10.1109/TIE.2018.2813991.
- [18] G. F. H. Beng, X. Zhang, and D. M. Vilathgamuwa, "Sensor fault-resilient control of interior permanent-magnet synchronous motor drives," *IEEE/ASME Transactions on Mechatronics*, vol. 20, no. 2, pp. 855–864, Apr. 2015, doi: 10.1109/TMECH.2014.2311126.
- [19] S. K. Kommuri, M. Defoort, H. R. Karimi, and K. C. Veluvolu, "A robust observer-based sensor fault-tolerant control for PMSM in electric vehicles," *IEEE Transactions on Industrial Electronics*, vol. 63, no. 12, pp. 7671–7681, Dec. 2016, doi: 10.1109/TIE.2016.2590993.
- [20] B. Cai, Y. Zhao, H. Liu, and M. Xie, "A data-driven fault diagnosis methodology in three-phase inverters for PMSM drive systems," *IEEE Transactions on Power Electronics*, vol. 32, no. 7, pp. 5590–5600, Jul. 2017, doi: 10.1109/TPEL.2016.2608842.




- [21] B. Hafez, A. S. Abdel-Khalik, A. M. Massoud, S. Ahmed, and R. D. Lorenz, "single-sensor-based three-phase permanent-magnet synchronous motor drive system with Luenberger observers for motor line current reconstruction," *IEEE Transactions on Industry Applications*, vol. 50, no. 4, pp. 2602–2613, Jul. 2014, doi: 10.1109/TIA.2013.2296625.
- [22] G. Zhang, H. Zhou, G. Wang, C. Li, and D. Xu, "Current sensor fault-tolerant control for encoderless IPMSM drives based on current space vector error reconstruction," *IEEE Journal of Emerging and Selected Topics in Power Electronics*, vol. 8, no. 4, pp. 3658–3668, Dec. 2020, doi: 10.1109/JESTPE.2019.2941255.
- [23] Y. Liu, M. Stettenbenz, and A. M. Bazzi, "Smooth fault-tolerant control of induction motor drives with sensor failures," *IEEE Transactions on Power Electronics*, vol. 34, no. 4, pp. 3544–3552, Apr. 2019, doi: 10.1109/TPEL.2018.2848964.
- [24] M. Manohar and S. Das, "Current sensor fault-tolerant control for direct torque control of induction motor drive using flux-linkage observer," *IEEE Transactions on Industrial Informatics*, vol. 13, no. 6, pp. 2824–2833, Dec. 2017, doi: 10.1109/TII.2017.2714675.
- [25] B. Tabbache, N. Rizoug, M. E. H. Benbouzid, and A. Kheloui, "A control reconfiguration strategy for post-sensor FTC in induction motor-based EVs," *IEEE Transactions on Vehicular Technology*, vol. 62, no. 3, pp. 965–971, Mar. 2013, doi: 10.1109/TVT.2012.2232325.
- [26] M. Jannati, N. R. N. Idris, and M. J. A. Aziz, "Indirect rotor field-oriented control of fault-tolerant drive system for three-phase induction motor with rotor resistance estimation using EKF," *TELKOMNIKA Indonesian Journal of Electrical Engineering*, vol. 12, no. 9, pp. 6633–6643, Sep. 2014, doi: 10.11591/telkomnika.v12i9.6309.
- [27] M. H. N. Razali, J. M. Lazi, Z. Ibrahim, M. H. N. Talib, and F. A. Patakor, "Sliding mode control with observer for permanent magnet synchronous machine drives," *Indonesian Journal of Electrical Engineering and Computer Science*, vol. 25, no. 1, pp. 89–97, Jan. 2022, doi: 10.11591/ijeecs.v25.i1.pp89-97.
- [28] A. S. S. Saari and D. Ishak, "Design and fault tolerant analysis of five-phase permanent magnet synchronous motor," *Indonesian Journal of Electrical Engineering and Computer Science*, vol. 16, no. 3, p. 1115, Dec. 2019, doi: 10.11591/ijeecs.v16.i3.pp1115-1125.
- [29] M. Khayamy and H. Chaoui, "Current sensorless MTPA operation of interior PMSM drives for vehicular applications," *IEEE Transactions on Vehicular Technology*, vol. 67, no. 8, pp. 6872–6881, Aug. 2018, doi: 10.1109/TVT.2018.2823538.
- [30] R. Li, Z. Wu, and X. Li, "Review on fault diagnosis and active fault tolerant control of permanent magnet synchronous motor drive system," *Journal of Applied Science and Engineering (Taiwan)*, vol. 24, no. 2, pp. 185–205, 2021, doi: 10.6180/jase.202104\_24(2).0008.

## BIOGRAPHIES OF AUTHORS



**Sankhadip Saha**    received an undergraduate degree in Electrical Engineering from Maulana Abul Kalam Azad University of Technology, India, in 2005 and a postgraduate degree in Control & Instrumentation from Maulana Abul Kalam Azad University of Technology, India, in 2007. Currently, he is Assistant Professor in the Electrical Engineering Department, Netaji Subhash Engineering College, Kolkata, India. Presently he is pursuing Ph.D degree at Maulana Abul Kalam Azad University of Technology, India. His research includes the signal processing and control system in power electronics and machine drives. He can be contacted at email: sankhadip.saha@nsec.ac.in.



**Dr. Urmila Kar**    is a Professor and Head of the Department of Education and Management of National Institute of Technical Teachers' Training and Research (NITTTR) Kolkata, India. She obtained her BE degree in Electrical Engineering from Regional Engineering College, Silchar and MEE degree with a specialization in Control System from Jadavpur University, Kolkata, India. She obtained her Doctoral degree in Engineering from Jadavpur University, Kolkata, India. Her research area includes nonlinear system dynamics and control, fuzzy logic control and engineering education. She can be contacted at email: urmilakar@nitttr.kol.ac.in.